

Pattern recognition based on HD-sEMG spatial features extraction for an efficient proportional control of a robotic arm

F. Nougarou^a, A. Campeau-Lecours^b, D. Massicotte^a, M. Boukadoum^c, C. Gosselin^b and B. Gosselin^d

^a Department of Electrical and Computing Engineering, University of Québec at Trois-Rivières, Québec, Canada

^b Department of Department of Mechanical Engineering, Laval University, Québec, Canada

^c Department of Computing Engineering, University of Québec at Montréal, Québec, Canada

^d Department of Electrical and Computing Engineering, Laval University, Québec, Canada

ARTICLE INFO

Article history:

Received 00 December 00

Received in revised form 00 January 00

Accepted 00 February 00

Keywords:

Pattern recognition

HD-sEMG

Spatial features

Spatial filtering

Sequential and proportionnal control

Linear regression

Assistive robotics

ABSTRACT

To enable an efficient alternative control of an assistive robotic arm using electromyographic (EMG) signals, the control method must simultaneously provide both the direction and the velocity. However, the contraction variations of the forearm muscles, used to proportionally control the device's velocity using a regression method, can disturb the accuracy of the classification used to estimate its direction at the same time. In this paper, the original set of spatial features takes advantage of the 2D structure of an 8×8 high-density surface EMG (HD-sEMG) sensor to perform a high accuracy classification while improving the robustness to the contraction variations. Based on the HD-sEMG sensor, different muscular activity images are extracted by applying different spatial filters. In order to characterize their distribution specific to each movement, instead of the EMG signals' amplitudes, these muscular images are divided in sub-images upon which the proposed spatial features, such as the centers of the gravity coordinates and the percentages of influence, are computed. These features permits to achieve average accuracies of 97% and 96.7% to detect respectively 16 forearm movements performed by a healthy subject with prior experience with the control approach and 10 movements by ten inexperienced healthy subjects. Compared with the time-domain features, the proposed method exhibits significant higher accuracies in presence of muscular contraction variations, requires less training data and is more robust against the time of use. Furthermore, two fine real-time tasks illustrate the potential of the proposed approach to efficiently control a robotic arm.

© xxxxxxxxxxxxxx. All rights reserved.

1. Introduction

Used on a daily basis by disabled persons, JACO, shown in Fig.1, is a 6 degrees-of-freedom (DOFs) robotic arm from Kinova Robotics with 3 flexible fingers controlled by a sensitive joystick [1,2]. However, more convenient controls must be developed for people unable to use the joystick; namely persons with damages to the motor system or neuromuscular disorders like cerebral palsy, spinal cord injury or stroke. This work develops an alternative control which simultaneously provides the direction and velocity of a robotic arm based on the forearm muscular signals. This approach is based exclusively on sEMG (surface Electromyography) electrodes.

Two approaches were investigated in past decades to control some devices based on EMG signals [4]: the classification [5,6] and the regression [7]-[10]. The classification can control many DOFs with high precision, but one DOF at the time (sequential control) meanwhile the proportional control decreases its accuracy [7,11]. The regression provides simultaneous (combination of DOFs) and proportional controls [7]-[10]. However, its control is inaccurate for more than 2 DOFs [4].

Because a large number of movements must be detected with high classification accuracy, the proposed control relies on a pattern recognition method [5,6] which uses extracted features from the EMG signals to feed a classifier. The recognized movements will be associated with the robot arm directions. At the same, a linear regression method [9,10] will be employed to associate the level of contraction (i.e. EMG amplitude) with the robot arm velocity. To do this without compromising the classification accuracy, an original set of features, chosen to be the more independent from the EMG amplitude as possible, is proposed. Doing so, the level of contraction could be varied to control the velocity without disturbing the recognition.

Many studies, based on sEMG electrodes placed at precise anatomical positions, were conducted to develop pattern recognition methods by extracting various kinds of features from EMG signals [12]-[16] while using different classifiers [12,17]. The set of the four time-domain (TD) features proposed in [12] is adopted as a benchmark owing to its robust and efficiency in discriminating movements. The features' choice has a greater impact than the classifier itself. A simple and stable LDA (Linear Discriminant Analysis) [17] results similar to more complex classifiers [12,17].

Increasingly used in biomedical research [18]-[22], high-density surface EMG electrodes (HD-sEMG), composed of equally spaced sEMG electrodes organized in lines and columns, were also used to achieve pattern recognition in many studies [23]-[33]. The HD-sEMG sensors allows to reach high classification accuracies for a large number of movements, particularly when the method is based on the TD features [30,32]. In [30], accuracies between 85–98% are achieved to find 13 movements using a HD-sEMG sensor and an average accuracy of 96.1% to recognize 20 movements is reached in [32] with 2 HD-sEMG sensors. However, since TD features are dependent on the amplitude, it does not meet our objectives. However, another interest in the HD-sEMG sensor lies in its 2D arrangement. Indeed, this 2D structure can provide maps (or images) of the muscular activities during a given task [26] and the spatial distribution of the muscular activity returns muscular strategies. In [21,22], the center of gravity displacements of the muscle activity image were used to characterize this muscle distribution. The spatial distribution obtained from HD-sEMG sensors is shown to differentiate forearm movements [26,29]: each movement having a different muscular image. The authors in [28] measure the variations in the images of the forearm muscles from 3 HD-sEMG sensors to recognize 9 movements with 95% accuracy. In [33], a recognition method achieves an accuracy of 89.3% to detect 8 forearm movements by directly providing each sample of a HD-sEMG image to a deep convolutional network. Then, the application of majority voting returns 99% of accuracy. The authors in [35] reaches an average classification accuracy of 86.63% to recognize 8 movements using spatial features based on histograms of oriented gradient and a SVM classifier. Finally, a multi-class proportional estimator based on common spatial pattern computed from HD-sEMG sensors was proposed in [34] to control a prosthesis in real-time. This 2D structure also allows the application of spatial filters of different orders [22,23]. The greater the increase in the spatial filter order, the greater the reduction of the crosstalk, and the more the measured signals reflect the behavior of the muscle layers close to the electrode [18,22].

Therefore, a HD-sEMG sensor makes it possible to observe the spatial distribution of different muscular depths.

Without direct information on amplitude, the proposed features characterize the spatial distribution of the forearm muscle activity images corresponding to different depths (spatial filters) [23]. As such, the classification method based on these original spatial features, namely the coordinates of the *centers of gravity* and the *percentages of influence*, becomes robust to amplitude variations. In Fig.1, these features are fed into a LDA to find 16 movements translated into robot motions. At the same time, a linear regression method uses the mean amplitude of signals to proportionally control the velocity of the robotic arm with the muscular contraction. Considering one healthy subject experienced with the EMG control approach and ten inexperienced subjects, the proposed spatial features and the TD features are compared under different conditions such as the variation or not of the muscular contractions. In addition, two real tasks with the robotic arm conducted by the experienced subject evaluate the proposed control that provides both the direction and the velocity simultaneously.

2. Proposed Pattern Recognition

To fully control the direction and the velocity of a robotic arm with a HD-sEMG sensor placed on the forearm, the proposed pattern recognition, depicted in Fig. 1, consists of two main phases: the learning and the estimation phase. The learning phase is an offline process in which the M known movements chosen by the user to control the robotic device are performed and used to fix the LDA coefficients \mathbf{z}^{LDA} and the parameters of the velocity control method, δ_m and ι_m , based on linear regression. During the estimation phase, at each instant w , these coefficients are used in real time to provide an estimated code of movement $\hat{C}_m[w]$ and a velocity $v_m[w]$ in order to control, at the same time, the direction and the velocity

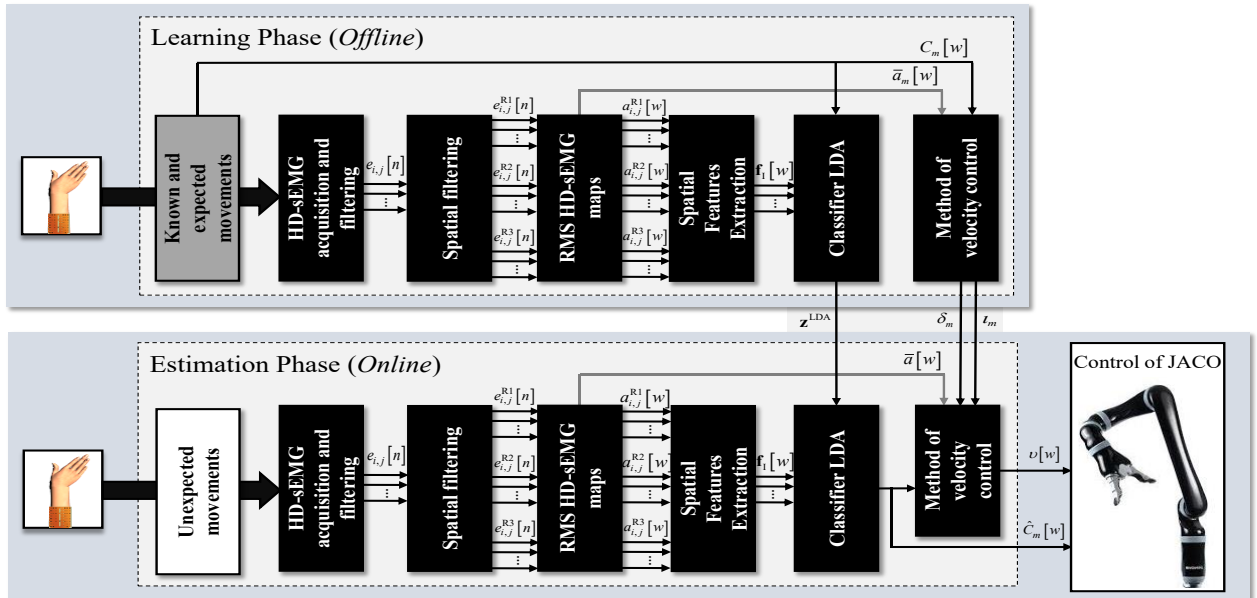


Fig. 1. Description of the proposed method of robotic arm control based on two main phases: learning and estimation.

of the robotic arm from unexpected movements. As shown in Fig.1, the proposed method takes strong advantage of the HD-sEMG sensor. At each 125ms, the monopolar signals from an 8×8 HD-sEMG sensor returns three different images of muscle activity obtained by applying three different spatial filters [22]. Each image is divided into sub-images of equal size in which two spatial features, robust to the variations of muscular contractions, are computed: the coordinates of the *center of gravity* and the *percentage of influence*. The following paragraphs detail each part of the method illustrated in Fig. 1.

2.1. HD-sEMG acquisition & spatial filtering

A HD-sEMG sensor of $N_i = 8$ rows and $N_j = 8$ columns of single sEMG electrodes is placed on a user's forearm to record the muscular activity during a given movement m of the wrist or the hand, with $m = 1, 2, \dots, M$ and M the number of gestures. The signal $e_{i,j}[n]$ of the electrode at row i and column j is the monopolar mode voltage between its position and the ground; with $i = 1, 2, \dots, N_i$, $j = 1, 2, \dots, N_j$ and $n = 1, 2, \dots, N$ where N is the number of samples with a sampling frequency of $F_s = 2048\text{Hz}$. To remove cardiac and power line interferences, a 30 to 450 Hz band-pass 4th order Butterworth filter and notch filters at 60Hz and its harmonics are applied to all signals.

To extract more information from the HD-sEMG sensor, $N_R = 3$ spatial filters are used at each sample n : the monopolar mode (1), the bipolar filter (2) and the inverse binominal filter (3) [22], recognized with superscripts «R1», «R2» and «R3». The signals $e_{i,j}^{R1}[n]$, $e_{i,j}^{R2}[n]$ and $e_{i,j}^{R3}[n]$ are different spatial selectivity or resolutions referring to different muscle depths [23].

$$e_{i,j}^{R1}[n] = e_{i,j}[n] \quad (1)$$

$$e_{i,j}^{R2}[n] = \text{sum} \begin{bmatrix} e_{i,j}[n] \\ -e_{i+1,j}[n] \end{bmatrix} \quad (2)$$

$$e_{i,j}^{R3}[n] = \text{sum} \begin{bmatrix} -e_{i-1,j-1}[n] & -2e_{i-1,j}[n] & -e_{i-1,j+1}[n] \\ -2e_{i,j-1}[n] & 12e_{i,j}[n] & -2e_{i,j+1}[n] \\ -e_{i+1,j-1}[n] & -2e_{i+1,j}[n] & -e_{i+1,j+1}[n] \end{bmatrix} \quad (3)$$

As shown in equations (2) and (3), it is not possible to apply: the bipolar filter (2) to the electrodes of the N_i^{th} row and the inverse binominal filter (3) to the electrodes of the rows 1 and N_i and of the columns 1 and N_j . For this reason, to obtain the same size for the signals $e_{i,j}^{R1}[n]$, $e_{i,j}^{R2}[n]$ and $e_{i,j}^{R3}[n]$, the equations (1) to (3) were computed for $i = 2, 3, \dots, N_i - 1$ and $j = 2, 3, \dots, N_j - 1$. For the rest of the description, the following variable changes is applied: $r = i - 1$ and $c = j - 1$ where $r = 1, 2, \dots, N_r$ and $c = 1, 2, \dots, N_c$ with $N_r = N_i - 2 = 6$ and $N_c = N_j - 2 = 6$. We define $s_{r,c}^{R1}[n] = e_{r+1,c+1}^{R1}[n] = e_{i,j}^{R1}[n]$, $s_{r,c}^{R2}[n] = e_{r+1,c+1}^{R2}[n] = e_{i,j}^{R2}[n]$ and $s_{r,c}^{R3}[n] = e_{r+1,c+1}^{R3}[n] = e_{i,j}^{R3}[n]$. Fig.2.a presents a set of 6×6 EMG signals for each resolution.

2.2. RMS HD-sEMG Maps

In the next step, muscular activity images or maps are constructed by computing RMS values of all signals resolutions defined in (1). For all rows r and columns c , the RMS values $a_{r,c}^{R1}[w]$, $a_{r,c}^{R2}[w]$ and $a_{r,c}^{R3}[w]$ are computed for each non-overlapped window w of 125ms from the signals $s_{r,c}^{R1}[n]$, $s_{r,c}^{R2}[n]$ and $s_{r,c}^{R3}[n]$ with $w = 1, 2, \dots, N_w$, the indexes of the N_w windows of 125ms. These muscular activity maps are created every 125ms as the extracted features and the estimated displacement and velocity. This process time is compatible with real-time use, because a pattern recognition process inferior to 300ms cannot be detected by the users [6].

Fig.2.b illustrates the RMS values based on processing windows of 125ms for the three resolutions. At a given window w , the RMS values are reorganized in rows and columns to obtain the three $N_r \times N_c$ images, as presented in Fig.2.c for all resolutions. In order to illustrate the difference between the three images obtained from the same HD-sEMG sensor by applying different spatial filters, a linear interpolation was used to add more details on the three 6×6 images in Fig.2.c. However, it is important to note that the proposed features extraction is based on uninterpolated images. The left image in Fig.2.c presents the positions of the 6×6 considered electrodes (black dots) from the 8×8 electrodes of the HD-sEMG sensor.

2.3. Spatial features extraction

The proposed set of features attempts to characterize the spatial distribution of the muscular images of each resolution without a direct dependence to the signals amplitudes. Towards this end, each image resolution of a given processing window w is first divided into $N_d = 9$ sub-images of equal size, where the integer $N_\varepsilon = \sqrt{N_d} = 3$ is the number of divisions per row and per column, as represented by the white lines in the images of Fig.2.c. As shown in this figure, the sub-images are organized as a $N_\varepsilon \times N_\varepsilon = 3 \times 3$ matrix indexed $\varepsilon_r = 1, 2, \dots, N_\varepsilon$ for the rows and with $\varepsilon_c = 1, 2, \dots, N_\varepsilon$ for the columns. Because in the present work $N_r = N_c$, each sub-image consists of $U = \lceil N_r / N_\varepsilon \rceil = \lceil N_c / N_\varepsilon \rceil = 2$ rows and columns of electrodes with the index vectors of the rows and columns $\mathbf{u}_r = [1, 2, \dots, U] = [1, 2]$ and $\mathbf{u}_c = [1, 2, \dots, U] = [1, 2]$. This means that, for the present case of image division, each sub-image contains 4 electrodes (4 black dots in each sub-image of the left image in Fig.2.c) where each electrode has its own RMS value $a_{r,c}^{R1}[w]$ (c.f. the monopolar map in Fig.2.c). Based on these definitions, the two proposed spatial features of the sub-image for row ε_r and column ε_c applied to the monopolar map, $a_{r,c}^{R1}[w]$, at each w are the following:

- The coordinates of the center of gravity (CG), $x_{\varepsilon_r, \varepsilon_c}^{R1}[w]$ (4) and $y_{\varepsilon_r, \varepsilon_c}^{R1}[w]$ (5), express the orientation of muscle activity of the given sub-image. The CG have been used in studies

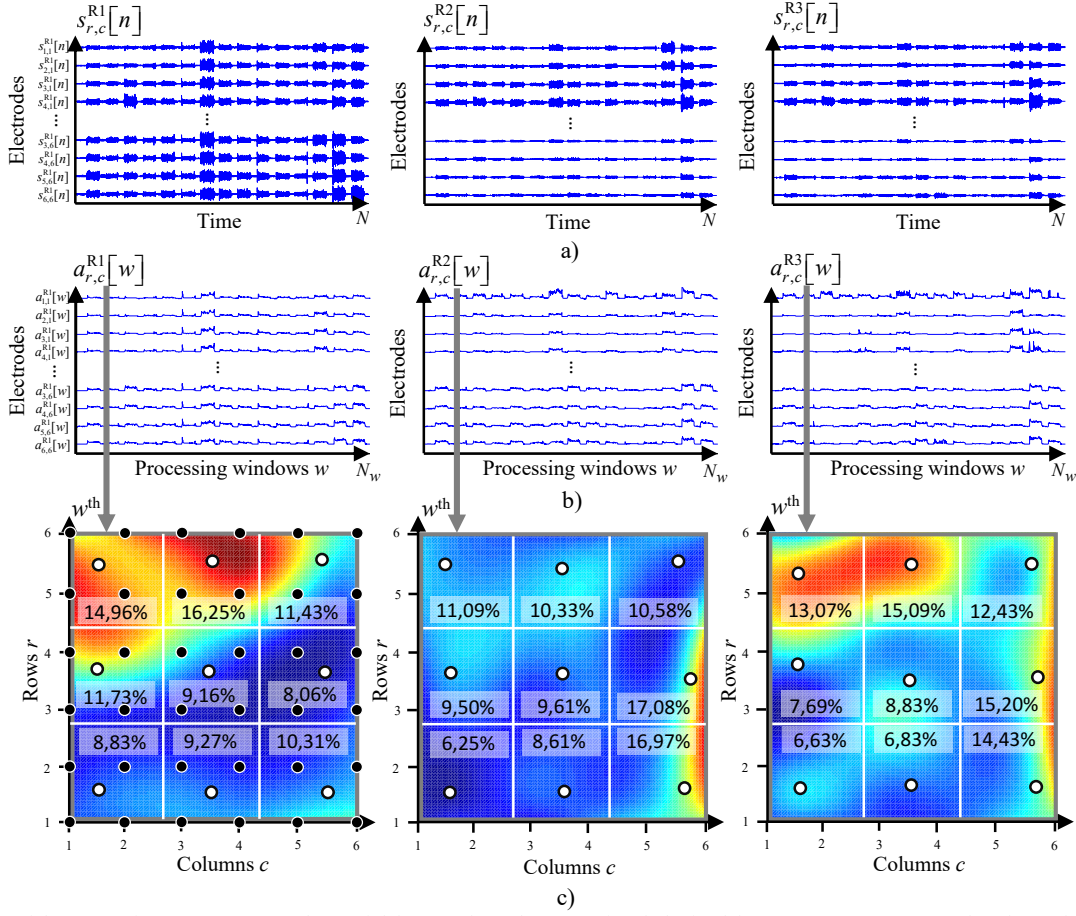


Fig. 2. Illustration of the successive steps to extract the spatial features from the EMG signal obtained from a HD-sEMG sensor placed on a forearm: a) example of the EMG electrode signals from the HD-sEMG sensor following the application of the different spatial filters (resolutions) for $M=16$ different movements, b) appearance of the EMG signals after the RMS computation in non-overlapped windows of 125ms for the three different resolutions, c) obtained 6x6 interpolated images of muscular distribution from the RMS values of the w^{th} processing window for all resolutions and obtained 9 sub-images and their corresponding center of gravity position and percentage of influence used as spatial features in the proposed method.

as [20,21] to characterize the muscular distribution, but has never been used as discriminant features in a pattern recognition context. Examples of the obtained centers of gravity appears in Fig.2.c for all resolutions (the white dots).

$$x_{\varepsilon_r, \varepsilon_c}^{R1}[w] = \frac{\text{mean}(r \times a_{r,c}^{R1}[w] \mid r = \mathbf{u}_r + (\varepsilon_r - 1)U, c = \mathbf{u}_c + (\varepsilon_c - 1)U)}{\text{mean}(a_{r,c}^{R1}[w] \mid r = \mathbf{u}_r + (\varepsilon_r - 1)U, c = \mathbf{u}_c + (\varepsilon_c - 1)U)} \quad (4)$$

$$y_{\varepsilon_r, \varepsilon_c}^{R1}[w] = \frac{\text{mean}(c \times a_{r,c}^{R1}[w] \mid r = \mathbf{u}_r + (\varepsilon_r - 1)U, c = \mathbf{u}_c + (\varepsilon_c - 1)U)}{\text{mean}(a_{r,c}^{R1}[w] \mid r = \mathbf{u}_r + (\varepsilon_r - 1)U, c = \mathbf{u}_c + (\varepsilon_c - 1)U)} \quad (5)$$

- Computed in each sub-image, the percentage of influence, $\beta_{\varepsilon_r, \varepsilon_c}^{R1}[w]$ (6), presents the influence each sub-image of a given image at the instant w , as in Fig.2.c for all resolutions.

$$\beta_{\varepsilon_r, \varepsilon_c}^{R1}[w] = 100 \times \frac{\text{mean}(a_{r,c}^{R1}[w] \mid r = \mathbf{u}_r + (\varepsilon_r - 1)U, c = \mathbf{u}_c + (\varepsilon_c - 1)U)}{\text{mean}(a_{r,c}^{R1}[w] \mid r = 1, 2, \dots, N_r, c = 1, 2, \dots, N_c)} \quad (6)$$

The coordinates of the centers of gravity (CG) and the percentages of influence are computed for all resolutions. At each instant w , a vector of features is constructed and used as input of the classifier. Based on these two features, three vectors

of features $\mathbf{f}_I^{\text{SP}}[w]$ (8), $\mathbf{f}_{II}^{\text{SP}}[w]$ (9) and $\mathbf{f}_{III}^{\text{SP}}[w]$ (10) (with «SP» for spatial features), are proposed and will be evaluated:

$$\mathbf{f}_I^{\text{SP}}[w] = \begin{bmatrix} x_{1,1}^{R1}[w], x_{1,2}^{R1}[w], \dots, x_{N_{\varepsilon_r}, N_{\varepsilon_c}}^{R1}[w], \dots \\ y_{1,1}^{R1}[w], y_{1,2}^{R1}[w], \dots, y_{N_{\varepsilon_r}, N_{\varepsilon_c}}^{R1}[w], \dots \\ \beta_{1,1}^{R1}[w], \beta_{1,2}^{R1}[w], \dots, \beta_{N_{\varepsilon_r}, N_{\varepsilon_c}}^{R1}[w] \end{bmatrix}^T \quad (7)$$

$$\mathbf{f}_I^{\text{SP}}[w] = [\mathbf{f}_{R1}^{\text{SP}}[w], \mathbf{f}_{R2}^{\text{SP}}[w], \mathbf{f}_{R3}^{\text{SP}}[w]]^T \quad (8)$$

$$\mathbf{f}_{II}^{\text{SP}}[w] = [\mathbf{f}_I^{\text{SP}}[w], \mathbf{f}_I^{\text{SP}}[w-1]]^T \quad (9)$$

$$\mathbf{f}_{III}^{\text{SP}}[w] = [\mathbf{f}_I^{\text{SP}}[w], \mathbf{f}_I^{\text{SP}}[w-1], \mathbf{f}_I^{\text{SP}}[w-2]]^T \quad (10)$$

The size of the features vector of $\mathbf{f}_I^{\text{SP}}[w]$ is equal to $N_{\mathbf{f}_I^{\text{SP}}} = N_f \times N_d \times N_R$, with $N_f = 3$ the number of features for a given sub-image. As shown in (9) and (10), the vectors of features $\mathbf{f}_{II}^{\text{SP}}[w]$ and $\mathbf{f}_{III}^{\text{SP}}[w]$ are based on the present and past values of $\mathbf{f}_I^{\text{SP}}[w]$. The sizes of those two sets of features are $N_{\mathbf{f}_{II}^{\text{SP}}} = 2N_{\mathbf{f}_I^{\text{SP}}}$ and $N_{\mathbf{f}_{III}^{\text{SP}}} = 3N_{\mathbf{f}_I^{\text{SP}}}$ respectively.

2.4. Classifier

The complexity of the proposed method represents an important issue because this pattern recognition should be implemented in an embedded processor and operated in real time. This complexity depends on the complexity of the used classifier. For this reason, the classifier considered herein is the LDA classifier, which, according to the literature, is the most popular for pattern recognition based on EMG, owing to its low complexity and stability [12]. During its learning phase, the LDA classifier computes the coefficients \mathbf{z}^{LDA} at all instant w , from the features and knowledges on the movement codes $C_m[w]$. In Fig.1, $\hat{C}_m[w]$ is the estimated movement code at each w from the features of unknown gestures, during the estimation phase. The LDA classifier's complexity directly depends on the size of the features vector.

2.5. Velocity Control based on linear regression

The proposed velocity control method of the robotic arm is based on linear regression [9]. It has to provide the velocity value $v[w]$ proportionally to the muscular contraction level of a given movement m in real time and simultaneously as the classification. To express the muscular contraction level at a given moment w with the HD-sEMG sensor, the mean of all RMS values of the image corresponding to the bipolar spatial filtering, noted $\bar{a}[w]$, is computed as shown in (11). The map of the bipolar spatial filtering was chosen because it is the most popular of the three used resolutions in EMG processing.

$$\bar{a}[w] = \text{mean}\left(a_{i,j}^{\text{R2}}[w] \mid r = 1, 2, \dots, N_r, c = 1, 2, \dots, N_c\right) \quad (11)$$

The proposed velocity control is based on one first order equation (12) per movement as followed for $m = 1, 2, \dots, M$:

$$v[w] = \delta^m \bar{a}[w] + \iota^m \quad (12)$$

where δ^m and ι^m , in Fig.1, are respectively the slope and the intercept values of the first order equation of the movement m , determined during the learning phase and used during the estimation phase. These two parameters require knowledges of the velocity range of the robotic arm $r_v = [\nu_{\min} \nu_{\max}]$ and the amplitude range of each executed movements $r^m = [\alpha_{\min}^m \alpha_{\max}^m]$ to be estimated. Because the range of amplitude r^m differs for all movements, δ^m and ι^m must be estimated for each of them. The velocity range, ν_{\min} and ν_{\max} is known because it is a parameter of the robotic arm.

In order to compute α_{\min}^m and α_{\max}^m , two kinds of contraction levels are performed for each movement during the EMG acquisition of the learning phase. Indeed, during this phase, the user executes each movement consecutively during 10s, where the first 7s are conducted with a moderate and comfortable strength whereas the last 3s are conducted with the maximum possible force without modifying the movement. Based on these two contraction levels per movement m , α_{\min}^m

and α_{\max}^m are defined as the average amplitude during the moderate contraction and during the maximum contraction (13), respectively. The amplitude contractions of a given movement m during the learning phase are represented by $\bar{\mathbf{a}}_m$, defined as $\bar{a}[w]$ in (11). $\bar{\mathbf{a}}_m^{\text{Mod.}}$ and $\bar{\mathbf{a}}_m^{\text{Max.}}$ are respectively the two distinct parts of $\bar{\mathbf{a}}_m$ representing the moderate and the maximum level of muscular contraction of the movement m .

$$\alpha_{\min}^m = \text{mean}\left(\bar{\mathbf{a}}_m^{\text{Mod.}}\right) \text{ and } \alpha_{\max}^m = \text{mean}\left(\bar{\mathbf{a}}_m^{\text{Max.}}\right) \quad (13)$$

Based on r_v and r^m , δ^m and ι^m can be easily identified and used to find the velocity $v[w]$, with (12), during the estimation phase base on the movement m detected by the LDA classifier.

3. Experiments, apparatus and Movements

In order to correctly evaluate the proposed method, two main approaches have been conducted:

















- One healthy 38 years old subject, trained to control a robotic arm with the developed method based on EMG signals of $M=16$ forearm movements and their level of contraction was considered to observe results under optimal operating conditions. Doing so, the mistakes due to bad movements made by inexperienced subjects are limited.
- Ten healthy 31.9 years old (on average with 9.67 years STD) volunteers without knowledge of the $M=10$ forearms movements were recruited to strengthen the analysis of the proposed method and to evaluate the impact of inexperienced subjects on the accuracy of the classification.

All participants provided their informed consent in accordance with the University Human Research Ethics Committee (CER-18-246-08-02.02).

Two main experiments were designed: (i) without the robotic arm for the experienced subject and the inexperienced subjects and (ii) with the robotic arm for the experienced subject only. The experiment without the device was designed to evaluate in depth the proposed methods using off-line and on-line data in comparison with the reference methods. All tested methods are defined in Table 2. The experiment with the robotic arm evaluates the ability of the proposed method to control it through two different tasks.

The same apparatus and processing structure were used in all experiments and for all subjects. One 8×8 HD sEMG sensor (64-channels sEMG, ELSCH064NM3, OT Bioelettronica; Torino, Italy) was placed on the posterior proximal part of the right forearm to record extensor muscles of the subjects. The sEMG signals were recorded in monopolar mode. One ground was placed on the ulnar styloid process of the wrist of each arm. The sensor and grounds were connected to the multichannel amplifier (EMG-USB2, OT Bioelettronica; Torino, Italy) which is in turn connected to the computer. A Matlab function (Matlab Release 2012b, The MathWorks, Inc.; Massachusetts, United States) allowed access to all electrodes data in real-time with a sampling rate of $F_s = 2048\text{Hz}$ and the methods were coded in Matlab. During the estimation phase, at each instant w , the Matlab program provides the robotic arm (JACO, Kinova Robotics; Montreal Canada) a direction and velocity command.

Table 1. The 16 human forearm movements and their associated robotic arm motions.

| Human forearm Movements | | Robotic Arm motions | Human forearm Movements | | Robotic Arm motions |
|-------------------------|---|---------------------------------------|-------------------------|--|---------------------|
| M1 |  Rest | Motion-less | M9 |  Wrist flexion and fingers Extension | y-displ. (+) |
| M2 |  Hand close | Hand close | M10 |  Fingers extension | y-displ. (-) |
| M3 |  Hand open | Hand open | M11 |  Pinch - thumb and little finger | x-rotation (+) |
| M4 |  Thumb, index and little extension | «Home» return to its initial position | M12 |  Pinch - thumb and ring finger | x-rotation (-) |
| M5 |  Wrist flexion | x-displ. (+) | M13 |  Pinch - thumb and middle finger | y-rotation (+) |
| M6 |  Wrist radial flexion | z-displ. (+) | M14 |  Pinch - thumb and index finger | y-rotation (-) |
| M7 |  Wrist ulnar flexion | z-displ. (-) | M15 |  Index finger crossed on the middle | Wrist rotation (+) |
| M8 |  Wrist Extension | x-displ. (-) | M16 |  Middle finger crossed on the index | Wrist rotation (-) |

For the experiments involving the experienced subject, the 16 movements of the Table 1 have been mapped with all the robot motions as intuitively as possible: the hand to open and close the robot hand, the wrist to control the x , y and z displacements, and the fingers to control the 3 rotations. There is one movement to return to the initial position (M4). If the rest movement (M1) is recognized, the robot remains in its previous position. Note that the HD-sEMG sensor detects the concentric and eccentric contractions to recognize the 16 movements. In their experiment, the ten inexperienced subjects performed the ten movements M1 to M10 of the Table 1.

4. Experiments without the robotic arm

4.1. Experiment of the experienced subject

The experienced user equipped with the HD-sEMG sensor had to perform an intensive experiment with all movements in real-time by following the indications on the computer screen. This data acquisition of more than three hours consists in a succession of learning sessions (LS) and estimation sessions (ES) depicted in Fig.3.a: a total of 6 LS and 5 ES detailed in the following sections. This experiment was designed to intensively compare the real-time recognition performance of the proposed method with reference methods successfully applied in [30,32], and to observe their robustness in time and in presence or absence of muscular contraction variations.

In each learning session, three successive learning phases (LP) were performed (see Fig.3.b). As explained in section 2.5 and exposed in Fig.3.d, in each learning phase, each movement was successively executed by the user during 10s with 7s of comfortable contraction and 3s of maximal contraction; a visual display showed to the user the movement to perform and its level. Because three learning phases were recorded per learning

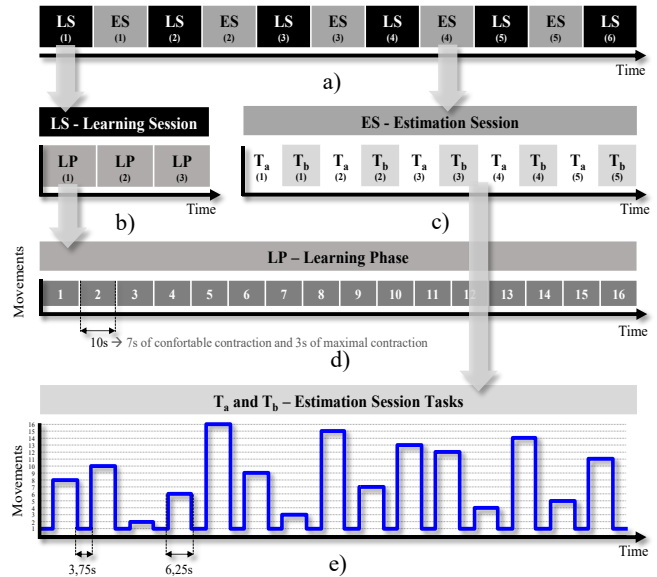


Fig.3. Description of the experiment without the robotic arm: a) general process as a succession of learning (LS) and estimation sessions (ES), b) learning session as a succession of learning phases (LP), c) estimation session as a succession of tasks T_a and tasks T_b , d) one learning phase during which each of 16 movements are executed successively during 10s and e) a given estimation session task in which each movement (except M1) are randomly executed during 6.25s and separated from each other by the movement M1 during 3.75s.

session, the impact in terms of recognition is observed whether 10, 20 or 30 seconds of data per movement are used to fix the LDA. Based on the succession of learning and estimation sessions as in Fig.3.a, the robustness in time of the proposed methods is evaluated: each learning session adjusting or not the LDA coefficients for the following estimation session.

In order to compare requested and executed gestures during the estimation sessions (see Fig.3.a), an interface was

developed to indicate the movements to perform in real-time. During each estimation session (ES), 10 estimation phases were successively performed through two different tasks: five phases *without muscular contraction constraint* (T_a in Fig.3.c) and five *with muscular contraction constraints* (T_b in Fig.3.c). Doing so, the robustness to muscular contraction variations could be observed. Indeed, in the task T_a , the user must perform the movement of the screen without any constraint. In the task T_b , in addition to performing the same movement as requested, *the user must vary the muscular contraction*, presented on the screen in real-time, *from minimum to the maximum levels*. As in shown Fig.3.e, all movements, except M1, appear during 6.25s in a random order and are separated by 3.75s of the rest.

The time-domain (TD) features [12], composed of the mean absolute value (MV), the zero-crossings (ZC), the slope sign changes (SC) and the waveform length (WL), demonstrated their efficiency and robustness. Considering the bipolar mode (noted by «R2»), these features were computed from $s_{r,c}^{R2}[w]$ defined in section 2.1 for all windows w , row r and column c . It results $MV_{r,c}^{R2}[w]$, $ZC_{r,c}^{R2}[w]$, $SC_{r,c}^{R2}[w]$ and $WL_{r,c}^{R2}[w]$. Similarly, the TD features were also computed from the $s_{r,c}^{R1}[w]$ and $s_{r,c}^{R3}[w]$. Two versions of the TD features were considered as reference methods: one based on the commonly used bipolar mode, $\mathbf{f}_I^{\text{TD}}[w] = \mathbf{f}_{R2}^{\text{TD}}[w]$ (14), and $\mathbf{f}_{II}^{\text{TD}}[w]$ (15) based on the three defined resolutions.

$$\mathbf{f}_I^{\text{TD}}[w] = \mathbf{f}_{R2}^{\text{TD}}[w] = \begin{bmatrix} [MV_{1,1}^{R2}[w], \dots, MV_{N_r, N_c}^{R2}[w], \dots] \\ [ZF_{1,1}^{R2}[w], \dots, ZF_{N_r, N_c}^{R2}[w], \dots] \\ [SC_{1,1}^{R2}[w], \dots, SC_{N_r, N_c}^{R2}[w], \dots] \\ [WL_{1,1}^{R2}[w], \dots, WL_{N_r, N_c}^{R2}[w]] \end{bmatrix}^T \quad (14)$$

$$\mathbf{f}_{II}^{\text{TD}}[w] = [\mathbf{f}_{R1}^{\text{TD}}[w], \mathbf{f}_{R2}^{\text{TD}}[w], \mathbf{f}_{R3}^{\text{TD}}[w]]^T \quad (15)$$

The size of $\mathbf{f}_I^{\text{TD}}[w]$ is $N_{\mathbf{f}_I^{\text{TD}}} = N_f \times N_r \times N_c$, with $N_f = 4$ the number of features for a given electrode and the size of $\mathbf{f}_{II}^{\text{TD}}[w]$ is $N_{\mathbf{f}_{II}^{\text{TD}}} = N_{\mathbf{f}_I^{\text{TD}}} \times N_R$. The five methods compared in this experiment are presented in the Table 2.

4.2. Experiment of the inexperienced subjects

To avoid the fatigue effect on the inexperienced subjects, a light version of the experience described in Fig.3 was built for the ten participants. In this experiment, only one learning session (LS) with two learning phases (LP) with 10 seconds for each of the 10 movements (M1 to M10 of the Table 1) was performed. During the unique estimation session (ES), 4 estimation phases were successively performed through two different tasks: two phases without muscular contraction constraint (T_a in Fig.3.c) and two with muscular contraction constraints (T_b in Fig.3.c). In these tasks, each movement has to be realized during 20 seconds. The accuracy results of SP_{II} and TD_{II} (Table 2) obtained during this estimation session were compared with and without muscular contraction constraint. A

Table 2. Tested classification methods in experiments without robotic arm in function of the set of features.

| Methods | Descriptions |
|------------|---|
| SP_I | Proposed method based on the features set $\mathbf{f}_I^{\text{SP}}[w]$ (8) |
| SP_{II} | Proposed method based on the features set $\mathbf{f}_{II}^{\text{SP}}[w]$ (9) |
| SP_{III} | Proposed method based on the features set of $\mathbf{f}_{III}^{\text{SP}}[w]$ (10) |
| TD_I | Time-domain method based on the set features $\mathbf{f}_I^{\text{TD}}[w]$ (14) |
| TD_{II} | Time-domain method based on the features set $\mathbf{f}_{II}^{\text{TD}}[w]$ (15) |

one-way repeated ANOVA was performed on obtained accuracies. The statistical significance was set at $p > 0.05$.

4.3. Results based on learning data of the experienced subject

Considering the intensive experiment based on the experienced subject, in total data from $N_{LP} = 18$ frames of learning phases were recorded. And, as shown in Fig.3.d, each of the 16 movements was performed during 10s for a given frame of learning phase. Those frames of data are used to evaluate and compare the classification methods of the Table 2 using the cross-validation strategy [30]. The cross-validation is performed by dividing the N_{LP} frames in two groups: N_L^{cross} frames, with $1 \leq N_L^{\text{cross}} < N_{LP}$, to perform the learning process of the methods and $N_E^{\text{cross}} = N_{LP} - N_L^{\text{cross}}$ frames to carry out their estimation process. To observe the impact of the number of the 10s learning frames to adjust the LDA coefficients, several sizes of cross-validation group are considered: $N_L^{\text{cross}} = 1, 2, \dots, N_{LP} - 1$. For each value of N_L^{cross} , several combinations of frames are possible. For this reason, a maximum of 100 randomly chosen combinations is simulated. Fig.4 presents the mean percentage error for recognizing the 16

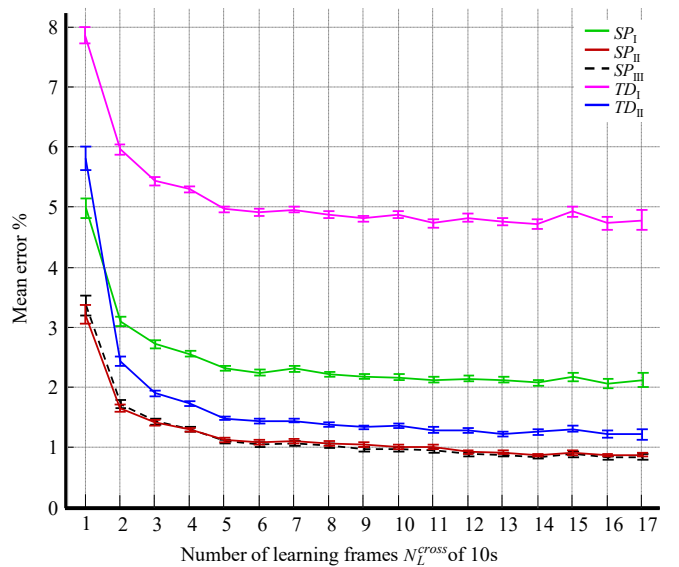


Fig.4. Mean error percentage obtained from the experienced subject based on number of learning frames of 10s, N_L^{cross} for pattern recognition methods based on features extractions depicted in Table 1 with an LDA classifier.

Table 3. Size of features vectors in function of the used method

| Methods | Size of the features vector used as LDA input |
|------------|---|
| SP_I | $N_{f_I^{SP}} = N_f \times N_d \times N_R = 3 \times 9 \times 3 = 81$ |
| SP_{II} | $N_{f_{II}^{SP}} = 2 \times N_f \times N_d \times N_R = 2 \times 3 \times 9 \times 3 = 162$ |
| SP_{III} | $N_{f_{III}^{SP}} = 3 \times N_f \times N_d \times N_R = 3 \times 3 \times 9 \times 3 = 243$ |
| TD_I | $N_{f_I^{TD}} = N_f \times N_r \times N_c = 4 \times 6 \times 6 = 144$ |
| TD_{II} | $N_{f_{II}^{TD}} = N_f \times N_r \times N_c \times N_R = 4 \times 6 \times 6 \times 3 = 432$ |

movements of N_E^{cross} 10s frames according to N_L^{cross} 10s frames per movement to carry out the learning process.

Based on Fig.4, the following observations can be made. The proposed methods SP_{II} and SP_{III} , based on spatial features and the LDA classifier, obtain the best results in term of error percentage for recognizing 16 movements: from an approximately 3.3% error with 1 learning frame to less than 1% error with more over 8 learning frames. Method TD_{II} , which extracts the TD features from signals based on three different types of spatial filtering (see section 2.1), returns a percentage of error that is close to but higher than SP_{II} and SP_{III} , except for 1 learning frame where TD_{II} obtains more than 5.5% error. Furthermore, as shown in Table 3, the proposed method SP_{II} has smaller feature vectors than the methods SP_{III} and TD_{II} . This observation is relevant since the complexity of the LDA classifier depends directly upon the size of the feature vector. The complexity of a pattern recognition system based on the proposed method SP_{II} is less complex than one based on the method TD_{II} (more than 2.5 time less complex) and returns better performances for recognizing 16 movements. Method TD_I , used in [30,32], returns the worst performance for recognizing 16 movements, obtaining greater than 4.5% error. Method SP_I , based on spatial distribution features, which has a small features vector size of 81, returns better performance than method TD_I for finding 16 movements (up to an error of 2%).

4.4. Estimation results for the experienced subject

As indicated in section 4.1, a methodology was developed to evaluate the methods of Table 2 in real-time execution, under presence or absence of contraction variations and in function of time of use. Fig.5 presents the results obtained from simulated methods when a relearning occurs every ten estimation phases as described in section 4.1. Because each estimation phase (see section 4.1) takes exactly 2.6 minutes, a learning session is made around every 26 minutes. Three learning phases are performed during each learning session. For this reason, Fig.5.a, Fig.5.b and Fig.5.c, respectively, present the percentage of error during the estimation phase when 10, 20 or 30 seconds of data per movement are used to fix the LDA coefficients.

Regarding the results without constraints (constant amplitude of the EMG signals), methods SP_{II} and SP_{III} attain a mean error of about 3% for recognizing 16 movements in real-time context. Method SP_{II} outperforms method TD_{II} when only 10s (in Fig.5.a) and 20s (in Fig.5.b) per movement are used in the learning session. However, as shown in Fig.5.c, for 30s per movement to fix the LDA classifier, method TD_{II} returns close results compared with SP_{II} and SP_{III} . Method SP_{II} is the best version of the proposed methods and, in addition to attaining the smallest mean error percentage for recognizing 16 movements, it offers the major advantage of using a small number of learning data for performing well compared with method TD_{II} .

Considering the results with contraction variations during the movements' execution, method TD_{II} returns 3% more error than without this constraint whereas method SP_{II} obtained similar results with or without the muscular contraction constraint. The proposed method based on features presents a robustness to the amplitude variation of the EMG signals. Therefore, it can allow a simultaneous and efficient control of a device direction and velocity from muscular activity.

Fig.6 shows the mean percentage error in the recognition of 16 movements based on the successive estimation sessions of the experiment, with and without the muscular contraction constraints, when a learning session has been processed before

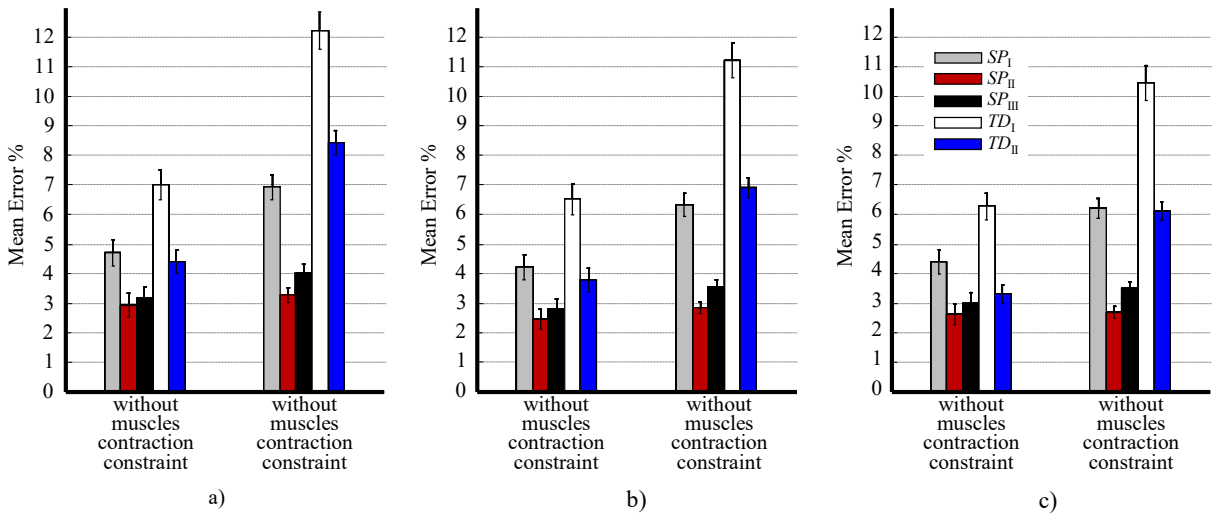


Fig.5. Mean error percentage obtained from the experienced subject based on two real-time conditions: to perform a movement without muscles contraction constraint (task T_a) or with muscles contraction variations (task T_b). These results are obtained by following the process described in Fig. 3 for the 5 methods of the Table 2 during the estimation phase when 10 a), 20 b) or 30 c) seconds of data per movement are used to fix the LDA coefficients during the learning sessions.

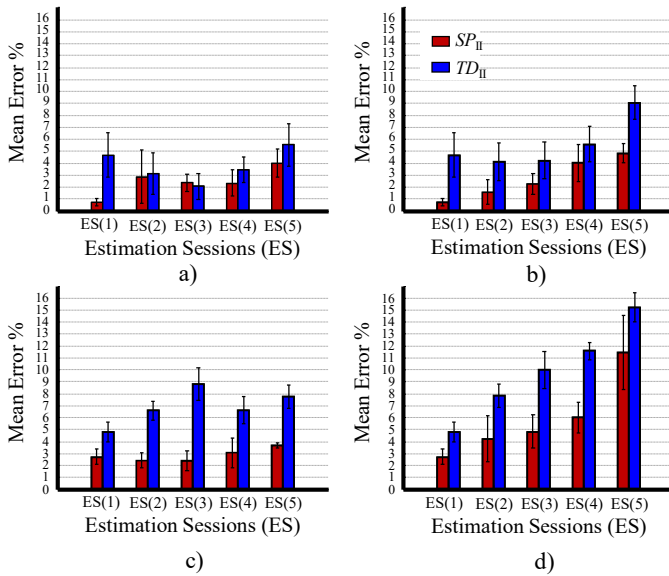


Fig. 6. Mean error percentage obtained from the experienced subject for methods SP_{II} and TD_{II} based on the considered estimation session (ES) a) with a learning session (LS) performed before each ES and without contraction constraint, b) with an LS performed before each ES and with contraction variations, c) with only the first LS used for all ES and without contraction constraint and d) with only the first LS used for all ES and with contraction variations. 30s of data per movement were used to fix the LDA coefficients during each learning session.

each estimation session, as shown in in Fig.6.a and Fig.6.c, and when learning has been achieved only before the first estimation session, for Fig.6.b and Fig.6.d. It is important to note that there is approximately 40 minutes between each estimation session (8 to 10 minutes for each learning session and 26 to 30 minutes for each estimation session) and approximately 3 hours and 15 minutes between the first and last estimation phase for Fig.6.b and Fig.6.d. As is the case for all methods, the greater the time gap between the update of the LDA classifier and an estimation phase, the greater the error of movement recognition. In Fig.6.c, this increase in error is more significant when there are variations in the muscle contractions. However, the error degradation is less important for method SP_{II} compared to method TD_{II} .

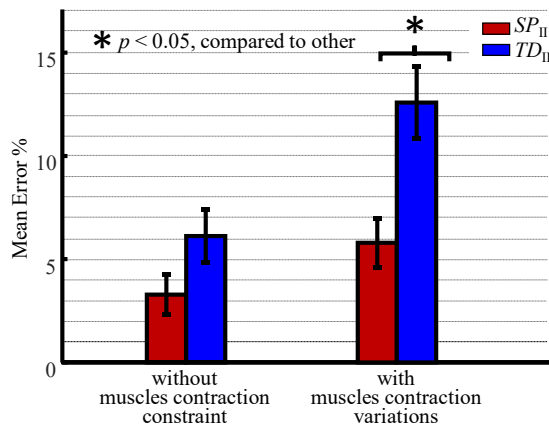


Fig. 7. Mean error percentage obtained from the ten inexperienced subjects based on two real-time conditions: to perform a movement without muscles contraction constraint (task T_a) or with muscles contraction variations (task T_b). These results are obtained by following the process described in section 4.2 for the methods SP_{II} and TD_{II} of the Table 2 during the estimation session.

4.5. Estimation results for the inexperienced subjects

Fig.7 show the overall mean error of classification obtained during the estimation session of the experimentation performed by the ten inexperienced subjects along two tasks (or conditions): one without muscles contraction constraint and one with muscles contraction variations (see section 4.2). Based on the same data for the learning phase used to fix their respective LDA classifier and the same data collected during the estimation phase, Fig.7 compared the results of the methods SP_{II} and TD_{II} presented in Table 2.

Without muscles contraction constrain, SP_{II} and TD_{II} respectively return $3.3\% \pm 0.9$ and $6.1\% \pm 1.3$ of mean error percentage (or 96.7% and 93.8% of mean accuracy percentage) to recognize 10 movements. As observed with the experienced subject, even if the method SP_{II} presents a better mean accuracy percentage, there is no significant difference with the method TD_{II} ($p = 0.08$). However, in presence of muscles contraction variations, SP_{II} and TD_{II} respectively obtain $5.8\% \pm 1.2$ and $12.6\% \pm 1.7$ of mean error percentage (or 94.2% and 87.4% of mean accuracy percentage) to find 10 movements. In this case, there is a significant difference between the results obtained with SP_{II} and TD_{II} ($p = 0.0014$). In addition, the method TD_{II} with muscle contraction variations also shows a significant difference with the methods SP_{II} and TD_{II} without muscles contraction constraint ($p = 3 \times 10^{-6}$ and $p = 0.0027$). Finally, there is no significant difference between the method SP_{II} with or without muscles contraction constraint ($p = 0.098$).

5. Experiments with the robotic arm

To present a first proof of concept of the proposed method's ability to control the robotic arm, two tasks of gradual difficulty, illustrated in Fig.8, were performed by the same experienced subject. Based on the results of section 4, method SP_{II} is used in this experiment to control the direction of the robotic arm.

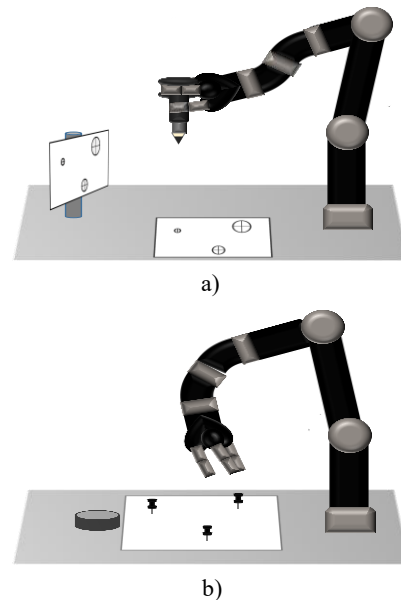


Fig.8. Illustration of two real-time tasks performed with the robotic arm controlled using the proposed method based on the spatial features extraction SP_{II} and speed control proportional to level of contraction: a) 3D pointing task with a pen and b) 3D fine manipulation task.

Table 4. Mean and standard deviation of time to perform the first task with robotic arm, of distance outside a given target and of total distance outside all targets based on robot velocity controls considered.

| Robot velocity controls | Mean (SD) time to realize the task (minute) | Mean (SD) distance outside a given target (millimeter) | | | | | | Total mean (SD) distance outside all targets (millimeter) |
|---------------------------------|---|--|-------------------|-------------------|-------------------|-------------------|-------------------|---|
| | | Horizontal position | | | Vertical position | | | |
| | | Target1 ø2.4cm | Target2 ø1.6cm | Target3 ø0.8cm | Target4 ø2.4cm | Target5 ø1.6cm | Target6 ø0.8cm | |
| Constant at 10cm/s | 2.08 (0.1) | 0 (0) | 1.6 (0.9) | 2.3 (0.6) | 2.7 (1.1) | 3.8 (0.7) | 5.6 (0.9) | 2.7 (1.9) |
| Constant at 20cm/s | 2.05 (0.2) | 0 (0) | 0.6 (0.3) | 3.2 (1.1) | 2.4 (1.1) | 5.2 (1.1) | 6.9 (1.3) | 3.0 (2.6) |
| Proportional to the contraction | 2.06 (0.1) | 0 (0) | 0 (0) | 0.8 (0.3) | 0.1 (0.1) | 0.4 (0.2) | 0.9 (0.6) | 0.3 (0.4) |

Our hypothesis is that the control of the robot velocity proportionally to the muscular contraction level is more intuitive and efficient than the use of constant velocities. Three kind of velocity controls were employed: one with the proposed method (proportional to contractions), one with a constant moderate velocity (10cm/s) and one with a constant high velocity (20cm/s). The robotic arm is controlled as follows: the pattern recognition method based on SP_{II} controls the direction with the estimated movements of Table 1 and the muscular contraction of a given movement proportionally controls its velocity. This approach is possible because the proposed pattern recognition method is robust to EMG amplitude variations.

The first task is a 3D pointing at circle targets of different sizes. A custom device was designed to hold the pen firmly and to absorb the shocks on the pen during vertical directions with a spring. As shown in Fig.8.a, six targets are pointed at: three on a horizontal plan and three others on a vertical plan placed in front of the robot at a slight angle to increase difficulty. On each plan, the three targets have a diameter of 0.8, 1.6 and 2.4 cm, respectively. For each trial, the robot hand is placed at its initial position reached with the «home» movement (M4 in Table 1) and the recorded time begins at its first move. During all trials, the order of the targets is the same and the recorded time is stopped when the last target is pointed at. For a given target, if the mark made by the pen is outside the circle, the smallest distance between the pen mark and the circle was measured. 10 trials were performed for each velocity control made successively to avoid any kind of learning. The results in Table 4 show that the mean time for performing the task is similar for all velocity control approaches and that the smaller the target, the greater the error. However, using a velocity control based on the muscle contraction makes it is easier to point at the target correctly. Indeed, the total mean distance outside the targets is equal to 0.3mm with this approaches instead of 2.7mm and 3mm for constant velocities of 10cm/s and 20cm/s. To complete this 3D task, 9 movements were used: M1, M4, M5, M6, M7, M8, M9, M10 and M12. This experiment shows that the proposed control allows to efficiently achieve 3D tasks with a millimeter range accuracy.

The second experiment with the robot is a 3D task that consists of picking up three standard tacks and depositing them in a cylindrical container 5 cm in diameter. The position of the three tacks is clearly identified on a sheet placed on a cork board, and the container has been positioned at the edge this sheet as illustrated in Fig.8.b. At the beginning of the task, the robotic hand is located above the cylindrical container, after which each tack is picked up in the same order. Because this task requires finer motions, a constant slow velocity of 5cm/s

Table 5. Mean and standard deviation of time to perform the second task with robotic arm and percentage of success based on robot velocity controls considered.

| Robot velocity Controls | Mean (SD) time to realize the task (minute) | Percentage of success of the task (%) |
|-------------------------|---|---------------------------------------|
| Constant at 5cm/s | 2.67 (0.2) | 100 |
| Constant at 10cm/s | 2.1 (0.2) | 44.4 |
| Constant at 20cm/s | 2.2 (0.3) | 27.8 |
| Prop. to the contr. | 2.08 (0.1) | 100 |

was also tested. 6 trials were conducted for each velocity control. During each trial, the time to perform the task was recorded and the number of tacks successfully placed in the container was noted. As Table 5 shows, it was possible to move 100% of the tacks correctly when the velocity control was proportional to contraction and when the velocity was fixed to the slower value. However, the approach based on proportional velocity allows the task to be performed an average of 35s (0.59 min) faster than the low velocity. For this very accurate task, the results obtained for the velocities equal 10cm/s, and 20cm/s were very poor with respectively 44.4% and 27.8% of tacks correctly placed in the cylinder. In addition to calling for high precision of execution, this task required the repeated use of 15 out of 16 movements, all except the “Home” movement, M4.

6. Discussion

The main contribution of this article consists of proposing an original set of spatial features designed to perform high classification accuracy while improving the robustness of the classification against the variations of muscular contraction. Indeed, considering the prediction results obtained with the experienced healthy subject, average accuracies of about 97% was reached with the proposed method (SP_{II}) under the presence or the absence of the muscular contraction variations to recognize 16 movements, as shown in Fig.5.c. Based on the prediction results from the ten inexperienced subjects and the proposed features (SP_{II}), average accuracies of $96.7\% \pm 0.9$ and $94.2\% \pm 1.2$ were obtained to detect 10 movements, respectively under the presence or the absence of the muscular contraction variations, as illustrated in Fig.7. This difference between these two experimental conditions is not significant ($p = 0.098$), but certainly occurs because it is not so easy for inexperienced subjects to make a movement while controlling the change of muscle contraction. Besides, the subject, experienced to perform the 16 movements while varying their muscular

contraction, successfully controls the direction and velocity of a robotic arm in real-time with the proposed features (SP_{II}) as shown in section 5 with two challenging tasks. These real-time results represent a proof of concept of the proposed method to efficiently control a 6 degrees-of-freedom robotic arm using EMG signals. This robustness of the muscular contraction variation is clearly due to the fact that the proposed features takes advantage of the 2D structure of the HD-sEMG sensor to characterize the muscular distribution instead of the EMG signals amplitude, as it is the case for the TD features [12].

As shown in [30,32], the TD features applied to HD-sEMG sensor signals allows to reach high classification accuracies for a large number of movements. However, unlike the proposed spatial features, the TD features render the classification method more sensible to the variation of the muscular contractions. The experimentation performed by the ten inexperienced subjects demonstrates that the accuracy obtained by the TD features TD_{II} to find 10 movements decreases significantly from $93.8\% \pm 1.3$ to $87.4\% \pm 1.7$ (see Fig.7) when the muscular contraction is varied. The same conclusions are observed in the intensive experiment realized with the experienced subject to detect 16 movements. The accuracy of the TD features TD_I , similar to [30,32], decreases from about 94% to 89.5% with or without muscular constraints and the accuracy of the TD features TD_{II} , with spatial filters, decreases from about 97% to 94%. This sensitivity to the contractions variation is directly due to TD features that relies on the EMG signals' amplitudes. Besides, as seen in Fig.6 and addressed in [24], the TD features are also more sensible, than spatial features, to the time of use which incurs some amplitude variations due to the muscle fatigue. Another interest of the robustness to the muscular contraction variations appears when inexperienced subjects used the proposed method. Indeed, these subjects are more susceptible to realize their movements with an inconstant different amplitude. As shown in Fig.7, based on the same learning data, the proposed spatial reaches a better average accuracy even without contraction constraints than TD features: 96.7% against 93.8% to find 10 movements.

In addition to the proposed features designed to efficiently and simply characterize muscular distribution, by computing the centers of gravity in sub-images rather the entire muscular image as made in [20]-[24] and the percentage of influence, another contribution of the proposition is the use of spatial filters [23]. Besides, the performances comparison in Fig.5 of the methods TD_I , based on the classic bipolar mode, and TD_{II} , based on the 3 different images corresponding to 3 different spatial filters, depicts the merits of the spatial filtering inferred from a HD-sEMG sensor only, which permits to extract additional information from the same raw signals. Finally, as discussed in section 4.3 and 4.4, the pattern recognition based on the proposed spatial features also requires less learning data and reduces the computational complexity compared to when TD features are used.

In the present work, contrary to [30,32], no method of dimension reduction as PCA (Principal Component Analysis) has been applied. Because the proposed method fully takes advantage of the 2D structure of HD-sEMG sensors, the reduction of the number of electrodes is not an avenue for a practical or clinical solution. The idea consists in developing more convenient HD-sEMG sensors.

There is no clear diagnosis that makes it difficult for a patient to use the joystick of a robotic arm. It varies depending on the type and the severity of the conditions and, for this reason, there are different alternative ways to control the robotic arm. All alternative control approaches have their advantages and disadvantages according to the targeted person or the environment in which the method is employed. For example, efficient combinations of inertia measurement unit (IMU) and EMG sensors to control a robotic arm were proposed in [2,3,37,36]. This approach can become problematic for patients unable to properly and repetitively control their movements. Therefore, based on a small number of movements and a switch mode, contrary to the proposed method in this study, this alternative control requires more steps and time to realise complex tasks. In [38], the authors propose a brain-computer interface (BCI) using a non-invasive EEG (electroencephalogram) signals to reach and grasp an object with a robotic arm in 3D space. This impressive approach requires no body movement, which is a big advantage for people having damages to the motor system or neuromuscular disorders. However, BCI based on non-invasive permits a proportional and simultaneous control to realize simple tasks, and, even if the BCI techniques are constantly improving, the accuracy is not that high, the time response is not satisfactory and it is not reliable [38,39]. In addition to its performances already mentioned, the proposed method in this paper permits to achieve complex tasks with a robotic arm in real-time. This approach can also be used on other parts of the human body (shoulder, back, leg or calf) in order to adapt the control to the patient's condition. In addition, its robustness to the muscular contraction variations, already discussed, could significantly reduce the effects of spasms and tremors of patients. Finally, the proposed approach based on HD-sEMG sensors can be directly applied to EEG sensors as it is planned in our future works.

Based on the present results for an experienced subject and inexperienced subjects, a study currently uses the proposed method to provide an efficient biofeedback in order to improve the rehabilitation of the paralyzed or partially paralyzed arm of patients with stroke. In this case, several healthy people and patients are tested to observe the impact of the proposed method according to the targeted application. In the present study, the experiment with the robot arm is a concept of proof that demonstrate the potential of the proposed control to achieve fine tasks. But real-time tasks with robust psychometric properties and performed by several subjects would have a stronger significance. Based on methods with spatial features, future studies will also be conducted to analyze their behaviours when it is used by different kind of patients unable to use the joystick, to observe the impact of recurrent spasms on the recognition performances and to perform a simultaneous control rather than a sequential and proportional control.

7. Conclusion

To simultaneously control both the direction and the velocity of an assistive robotic arm using muscular activity, the proposed pattern recognition method uses a HD-sEMG sensor placed on the forearm to create images of muscular distribution of different resolutions from which the extracted original spatial

features are fed to the LDA classifier. Doing so, the impact of the amplitude variations of the EMG signals is substantially reduced. The muscular contraction level of a given movement can be used to proportionally control the velocity of the robotic arm without disturbing the recognition of the movement used at the same time to control its direction. Based on an experienced subject and ten inexperienced subjects, it was shown that the pattern recognition based on the proposed spatial features exhibits a smaller average percentage of error, requires less learning data, is significantly more robust to muscular contraction variations, is more robust to the time of use and has lower computational complexity. Furthermore, two fine real-time tasks performed by the experienced subject expose the potential of the proposed approach to efficiently control a robotic arm.

Acknowledgements

This work is supported in part by the ReSMIQ.

References

- [1] A. Campeau-Lecours, et al, "JACO Assistive Robotic Device: Empowering People With Disabilities Through Innovative Algorithms," 2016 Rehabilitation Engineering and Assistive Technology Society of North America (RESNA) annual conference, July 2016.
- [2] C. L. Fall, et al, "Intuitive wireless control of a robotic arm for people living with an upper body disability," IEEE EMBC conf., pp. 4399-4402, August 2015.
- [3] U. Côté-Allard, et al, "A convolutional neural network for robotic arm guidance using sEMG based frequency-features", IEEE/RSJ Int. Conf. on Intel. Robots and Systems, pp. 2464 – 2470, October 2016.
- [4] S. Amsuess, et al, "Context-Dependent Upper Limb Prosthesis Control for Natural and Robust Use," IEEE Trans Neural Syst Rehabil. Eng., Vol. 24, No. 7, pp. 744-53, July 2016.
- [5] M. Oskoei and H. Hu, "Myoelectric Control Systems – A survey," Biomedical Signal Processing and control, Vol. 2, pp. 275-94, 2007.
- [6] D. Farina, et al, "The Extraction of neural information from the surface EMG for the control upper-limb prostheses: emerging avenues and challenges," IEEE Trans Neural Syst Rehabil. Eng., Vol. 22, No. 4, pp. 797-809, July 2014.
- [7] A. Ameri, et al, "Real-Time, Simultaneous Myoelectric Control Using Force and Position-Based Training Paradigms," IEEE Trans. Biomed. Eng., Vol. 61, No. 2, pp. 279–84, February 2014.
- [8] A. Ameri, et al, "Real-Time, Simultaneous Myoelectric Control Using Visual Target -Based Training Paradigm," Biomed. Signal Processing and Control, Vol. 13, pp. 8–14, April 2014.
- [9] L. H. Smith, et al, "Evaluation of Linear Regression Simultaneous Myoelectric Control Using Intramuscular EMG," IEEE Trans. Biomed. Eng., Vol. 63, No. 4, pp. 737–46, April 2016.
- [10] J. M. Hahne, et al, "Linear and Nonlinear Regression Techniques for Simultaneous and Proportional Myoelectric Control," IEEE Trans Neural Syst Rehabil. Eng., Vol. 22, No. 2, pp. 269-79, March 2014.
- [11] E. Scheme and K. Englehart, "Training strategies for mitigating the effect of proportional control on classification in pattern recognition-based myoelectric control," J. Prosthet. Orthot., vol. 25, no. 2, pp. 76–83, Apr. 2013.
- [12] K. Englehart and B. Hudgins, "A robust, real-time control scheme for multifunction myoelectric control," IEEE Trans. Biomed. Eng., Vol. 50, No. 7, pp. 848–54, June 2003.
- [13] D. Farina and R. Merletti, "Comparison of algorithms for estimation of EMG variables during voluntary isometric contractions," Journal of Electromyogr. Kinesiol., Vol. 10, No. 5, pp. 337-349, October 2000.
- [14] A. Phinyomark, et al, "A Novel Feature Extraction for Robust EMG Pattern Recognition," Journal of Computing, Vol. 1, No. 1, pp. 71-80, December 2009.
- [15] D. Tkach, et al, "Study of stability of time-domain features for electromyographic pattern recognition," Journal of Neuroeng. Rehabil. , May 2010.
- [16] K. Englehart, et al, "Classification of the myoelectric signal using time-frequency based representations," Journal of Med. Eng. & Phys., Vol. 21, No. 6, pp. 431-8, July 1999.
- [17] L. J. Hargrove, et al, "A Comparison of Surface and Intramuscular Myoelectric Signal Classification," IEEE Trans. Biomed. Eng., Vol. 54, No. 5, pp. 847-53, May 2007.
- [18] D. F. Stegeman, et al, "High-density Surface EMG: Techniques and Application at Motor Unit Level," Journal of Biocyber. and Biomed. Eng., Vol. 32, No. 3, pp. 3-27, July 2012.
- [19] G. Drost, et al, "Clinical applications of high-density surface EMG: A systematic review," Journal of Electromyogr. Kinesiol., Vol. 16, No. 6, pp. 586-602, December 2006.
- [20] J. Abboud, et al, "Test-retest reliability of trunk motor variability measured by large-array surface electromyography," Journal of Manipulative Physiol. Ther., Vol. 38, No. 6, pp. 359-64, July 2015.
- [21] A. Samani, et al, "Active biofeedback changes the spatial distribution of upper trapezius muscle activity during computer work," Eur. J. Appl. Physiol., Vol. 110, No. 2, pp. 415-23, September 2010.
- [22] D. Farina, et al, "Selectivity of Spatial Filters for Surface EMG Detection from the Tibialis Anterior Muscle," IEEE Trans. Biomed. Eng., Vol. 50, No. 3, pp. 354-64, March 2003.
- [23] J. M. Hahne, et al, "Spatial filtering for robust myoelectric control," IEEE Trans. Biomed. Eng., Vol. 59, No. 5, pp. 1436-43, May 2012.
- [24] M. Jordanić, M. Rojas-Martinez, M. A. Mañanas, J. F. Alonso, and H. R. Marateb, "A novel spatial feature for the identification of motor tasks using high-density electromyography," Sensors (Switzerland), 2017.
- [25] A. Boschmann and M. Platzner, "Towards robust HD EMG pattern recognition: Reducing electrode displacement effect using structural similarity," IEEE EMBS conf., pp. 4547-50, 2014.
- [26] M. Rojas-Martinez, et al, "High-density surface EMG maps from upper-arm and forearm muscles," Journal of Neuro. eng. Rehabil. , December 2012.
- [27] X. Tang, Y. Liu and D. Sun, "Hand Motion Classification Using a Multi-Channel Surface Electromyography Sensor," Sensors, Vol. 12, No. 2, pp. 1130-47, January 2012.
- [28] A. Stango, et al, "Spatial Correlation of High Density EMG Signals Provides Features Robust to Electrode Number and Shift in Pattern Recognition for Myocontrol," IEEE Trans Neural Syst Rehabil. Eng., Vol. 23, No. 2, pp. 186-98, March 2015.
- [29] M. Gazzoni, et al, "Quantifying Forearm Muscle Activity during Wrist and Finger Movements by Means of Multi-Channel Electromyography," PLoS One, Vol. 9, No. 10, October 2014.
- [30] H. Daley, et al, "High density electromyography data of normally limbed and transradial amputee subjects for multifunction prosthetic control," Journal of Electromyogr. Kinesiol., Vol. 22, No. 3, pp. 478-84, June 2012.
- [31] D. Yi-Chun, et al, "Portable hand motion classifier for multi-channel surface electromyography recognition using grey relational analysis," Expert Syst. with Appl., Vol. 37, No. 6, pp. 4283-91, May 2010.
- [32] X. Zhang and P. Zhou, "High-Density Myoelectric Pattern Recognition Toward Improved Stroke Rehabilitation," IEEE Trans. Biomed. Eng., Vol. 59, No. 6, pp. 1649-57, June 2012.
- [33] W. Geng, et al, "Gesture recognition by instantaneous surface EMG images," Nature – Scientific Reports, 8 pages, November 2016.
- [34] S. Amsuess, et al, "A Multi-Class Proportional Myocontrol Algorithm for Upper Limb Prosthesis Control: Validation in Real-Life Scenario," IEEE Trans Neural Syst Rehabil. Eng., Vol. 23, No. 5, pp. 827-36, July 2016.
- [35] R. Islam, D. Massicotte, F. Nougrou et W. Zhu, "HOG and Pairwise SVMs for Neuromuscular Activity Recognition Using Instantaneous HD-sEMG Images ", New Circuits and Syst. Conf. 2018 (NEWCAS), Canada, Juin 2018, 4 pages.
- [36] C. L. Fall, et al, "Wireless sEMG-Based Body–Machine Interface for Assistive Technology Devices," IEEE journal of biomedical and health informatics, Vol. 21, No. 4, July 2017.
- [37] C. L. Fall, et al., "A Multimodal Adaptive Wireless Control Interface for People with Upper-Body Disabilities," IEEE ISCAS, Spetember 2017.
- [38] J. Meng, et al, "Noninvasive Electroencephalogram Based Control of a Robotic Arm for Reach and Grasp Tasks," Scientific Reports, Vol. 6, December 2016.
- [39] A. Athanasiou, et al, "Towards Rehabilitation Robotics: Off-the-Shelf BCI Control of Anthropomorphic Robotic Arms," BioMed Research International, August 2017.